From thermodynamics to geodynamics: An overview of the geophysical thermodynamics of phase relations

Craig R. Bina



Dept. of Earth and Planetary Sciences
Northwestern University
Evanston, Illinois, U.S.A.



Katedra geofyziky
Matematicko-fyzikální fakulta
Univerzita Karlova v Praze

přednášky na podzim 2011
2. lekce 19.10.

THE CLAPEYRON SLOPE

$$dG^{\phi} = -S^{\phi}dT + V^{\phi}dP + \sum_i \mu_i^{\phi} dN_i^{\phi}$$

Free energy, entropy, and volume vary with composition:

$$\left(\frac{\partial G^{\phi}}{\partial N_i^{\phi}}\right)_{P,T,N_{j\neq i}} = \mu_i^{\phi}$$

$$\left(\frac{\partial S^{\phi}}{\partial N_i^{\phi}}\right)_{P,T,N_{j\neq i}} = s_i^{\phi} = -\left(\frac{\partial \mu_i^{\phi}}{\partial T}\right)_{P,N_j}$$

$$\left(\frac{\partial V^{\phi}}{\partial N_i^{\phi}}\right)_{P,T,N_{j\neq i}} = v_i^{\phi} = \left(\frac{\partial \mu_i^{\phi}}{\partial P}\right)_{T,N_j}$$

One Component ($Fo = Mg_2SiO_4$): $N = 1$
Two Phases (α and β): $R = 2$

$$\mu_{Fo}^{\alpha}(P,T) = \mu_{Fo}^{\beta}(P,T)$$

$$\rightarrow \Delta\mu_{Fo}^{\alpha\rightarrow\beta}(P,T) = \mu_{Fo}^{\beta}(P,T) - \mu_{Fo}^{\alpha}(P,T) = 0$$

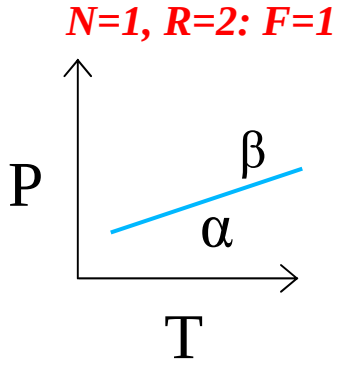
$$d\Delta\mu_{Fo}^{\alpha\rightarrow\beta} = \left(\frac{\partial \Delta\mu_{Fo}^{\alpha\rightarrow\beta}}{\partial T}\right)_P dT + \left(\frac{\partial \Delta\mu_{Fo}^{\alpha\rightarrow\beta}}{\partial P}\right)_T dP$$

$$= -\Delta s_{Fo}^{\alpha\rightarrow\beta} dT + \Delta v_{Fo}^{\alpha\rightarrow\beta} dP = 0$$

$$\rightarrow \frac{dP}{dT} = \frac{\Delta s_{Fo}^{\alpha\rightarrow\beta}(P,T)}{\Delta v_{Fo}^{\alpha\rightarrow\beta}(P,T)}$$

[Note that $\frac{dP}{dT}$ may vary with P and T.]

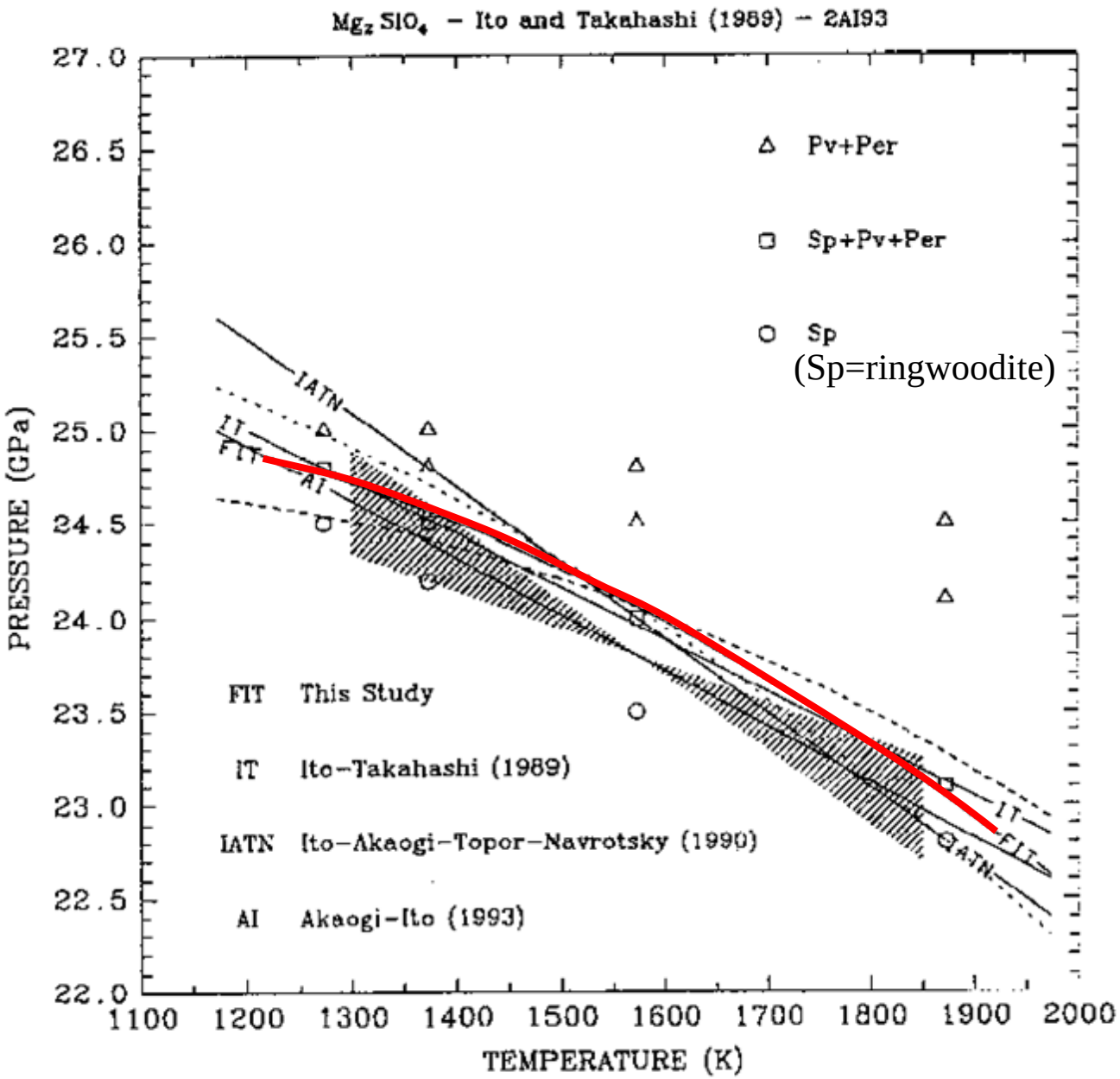
Clapeyron slopes are only defined for $N = 1$ and can be reasonably extended to $N > 1$ only for univariant ($F = 1$) cases.



$$dP / dT = \Delta S / \Delta V$$

(C.Bina, 9/2011)

Clapeyron Slopes Vary with Pressure and Temperature



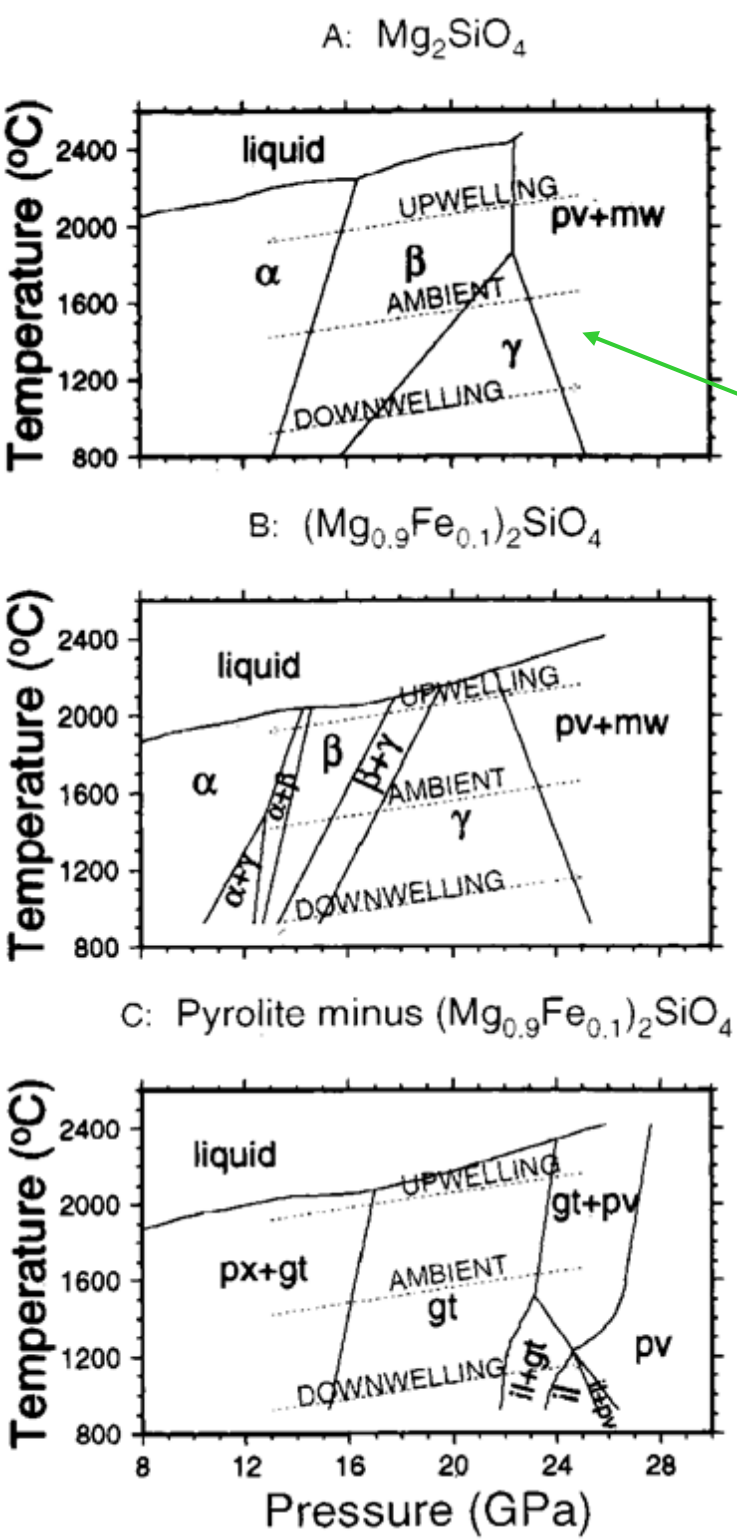
$$dP / dT = \Delta S(P,T) / \Delta V(P,T)$$

Phase diagram in *P-T* space for Mg_2SiO_4 showing transition of γ-spinel to perovskite + magnesiowüstite (periclase). Points are experimental data of *Ito and Takahashi* [1989]. Lines are (IT) boundaries fit by *Ito and Takahashi* [1989], (IATN) boundaries calculated by *Ito et al.* [1990], (AI) boundaries calculated by *Akaogi and Ito* [1993] with one-σ enthalpy uncertainties (hatchure), (FIT) boundaries calculated in this study using $\Delta H(T_0)$ of *Akaogi and Ito* [1993b] with one-σ enthalpy uncertainties (dashed).

(Figure 3 of Bina and Helffrich, 1994)

(C.Bina, 9/2011)

Clapeyron Slopes Defined Only for *N=1* Univariant Reactions



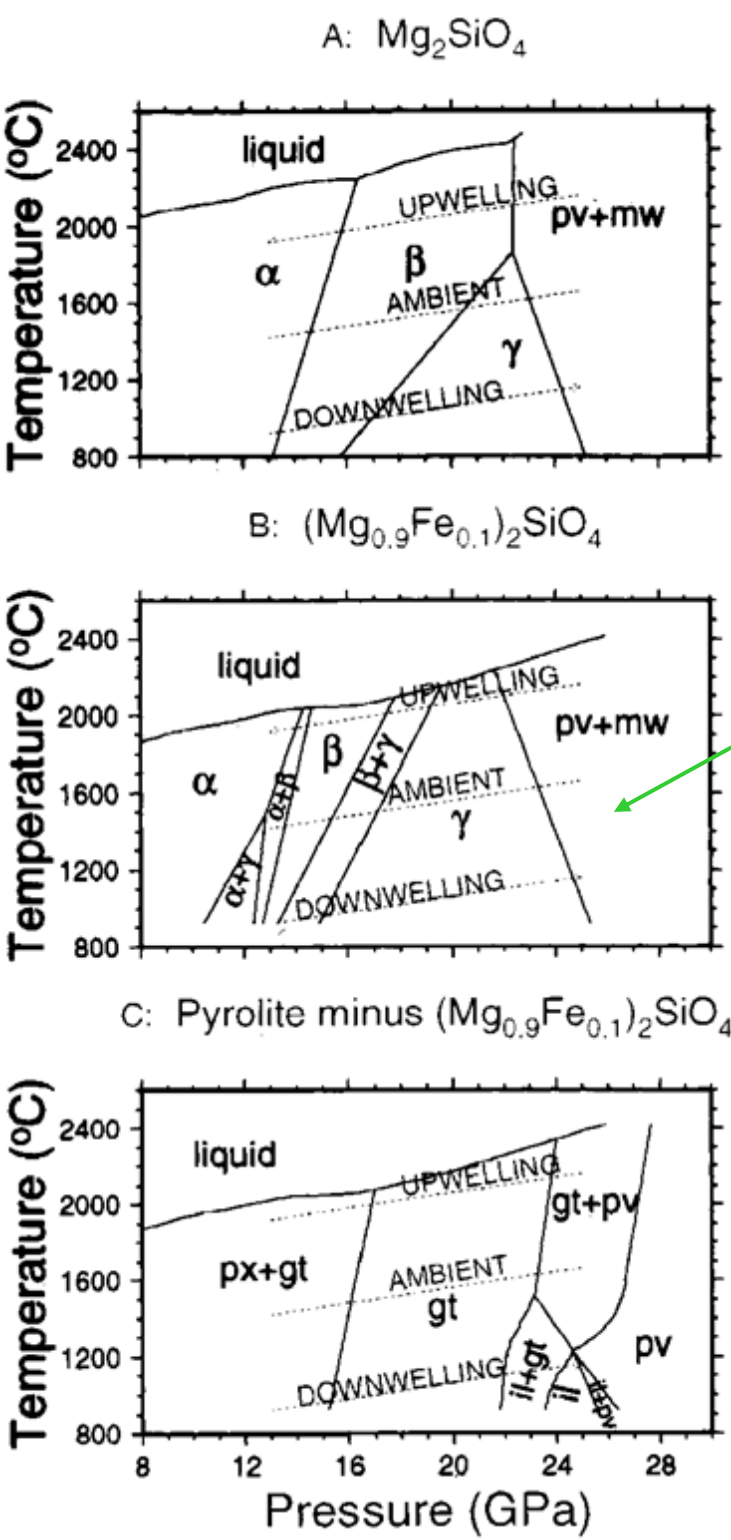
These univariant reactions have Clapeyron slopes.

Schematic phase diagrams for Mg_2SiO_4 olivine (**A**), $(Mg_{0.9}Fe_{0.1})_2SiO_4$ olivine (**B**), and pyroxene-garnet components (**C**), after *Gasparik* [I990] and *Ita and Stixrude* [1992]. Phases are olivine (α). modified spinel (β), spinel (γ). perovskite (*pv*), magnesiowüstite (*mw*), pyroxene (*px*), garnet (*gt*) . and ilmenite (*il*). Broken lines depict highlv schematic geotherms for ambient mantle, cold downwellings, and hot upwellings.

(Figure 1 of Bina and Liu, 1995)

(C.Bina, 9/2011)

Clapeyron Slopes Defined Only for *N=1* Univariant Reactions



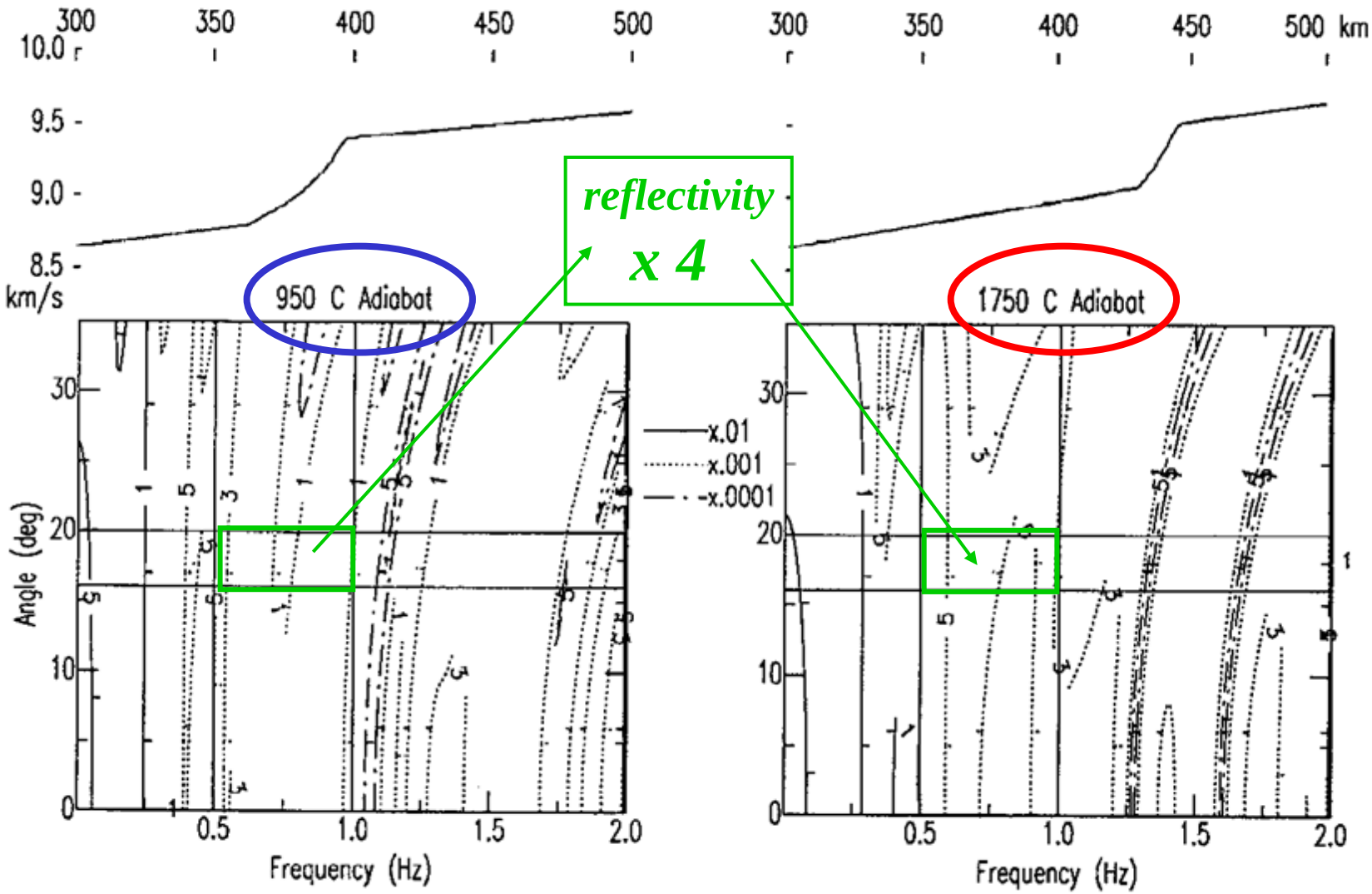
Most of these divariant reactions are nearly univariant (i.e., sharp), so perhaps we can define meaningful "effective" Clapeyron slopes for them.

Schematic phase diagrams for Mg_2SiO_4 olivine (**A**), $(Mg_{0.9}Fe_{0.1})_2SiO_4$ olivine (**B**), and pyroxene-garnet components (**C**), after *Gasparik* [I990] and *Ita and Stixrude* [1992]. Phases are olivine (α). modified spinel (β), spinel (γ). perovskite (*pv*), magnesiowüstite (*mw*), pyroxene (*px*), garnet (*gt*) . and ilmenite (*il*). Broken lines depict highlv schematic geotherms for ambient mantle, cold downwellings, and hot upwellings.

(Figure 1 of Bina and Liu, 1995)

(C.Bina, 9/2011)

Seismic Reflectivity of Finite-Width Phase Transitions



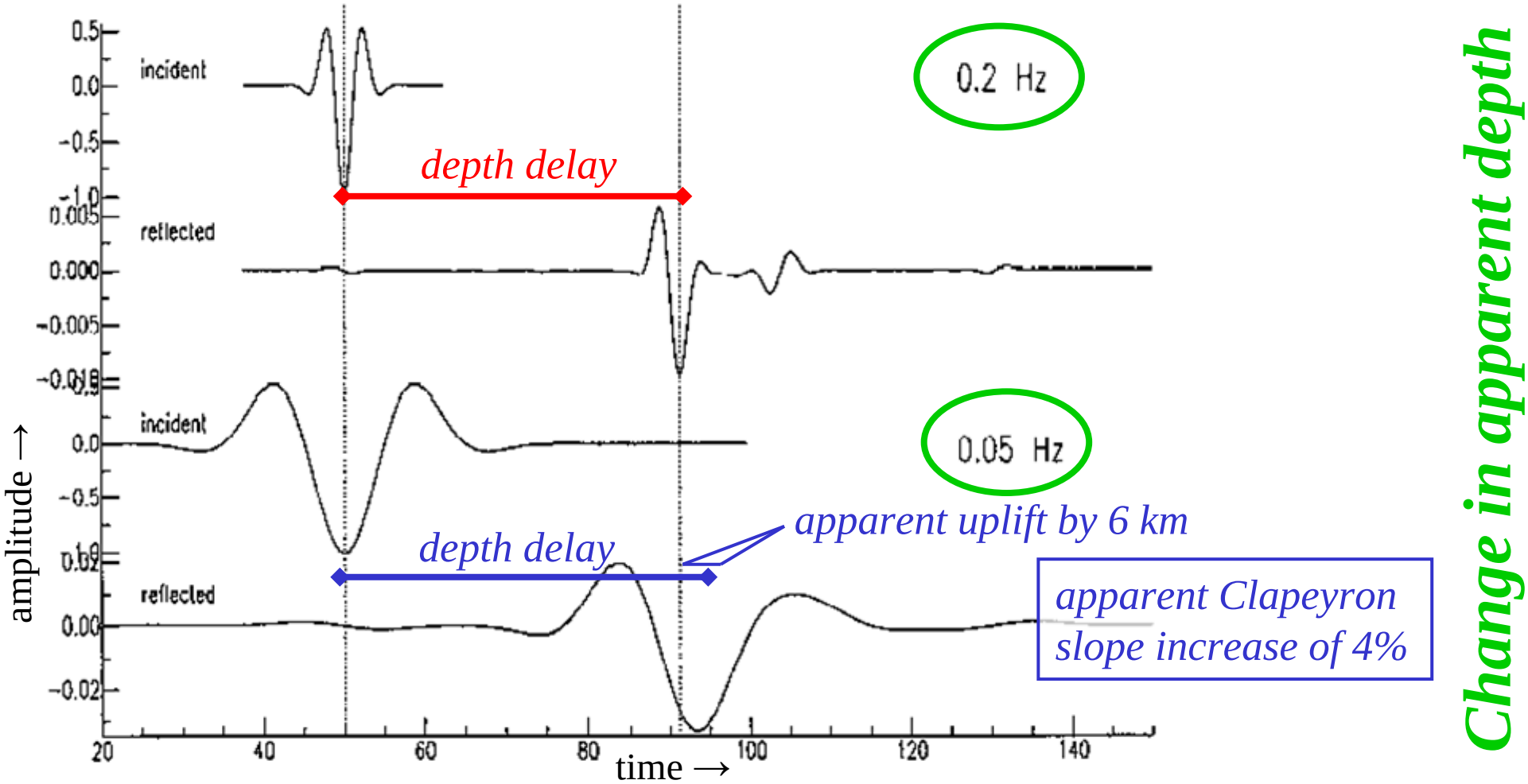
Change in reflected amplitude

Displacement amplitude P reflection coefficients computed for $a+\beta$ two-phase gradient zones for 950°C and 1750°C profiles. P velocity profiles shown at top of panels. Contours illustrate dependence of underside reflection coefficient on incidence angle and frequency, with the range relevant for $P'_{410}P'$ delimited by the lines (~18° and 0.5-1 Hz). Between 950°C and 1750°C the reflection coefficient varies by a factor of 2-4, potentially rendering the transformation invisible in the mantle when elevated to lower pressures by cooler temperatures. Conversely, the discontinuity sharpens and deepens at higher temperatures.

(Figure 2 of Helffrich and Bina, 1994)

(C.Bina, 9/2011)

Seismic Reflectivity of Finite-Width Phase Transitions

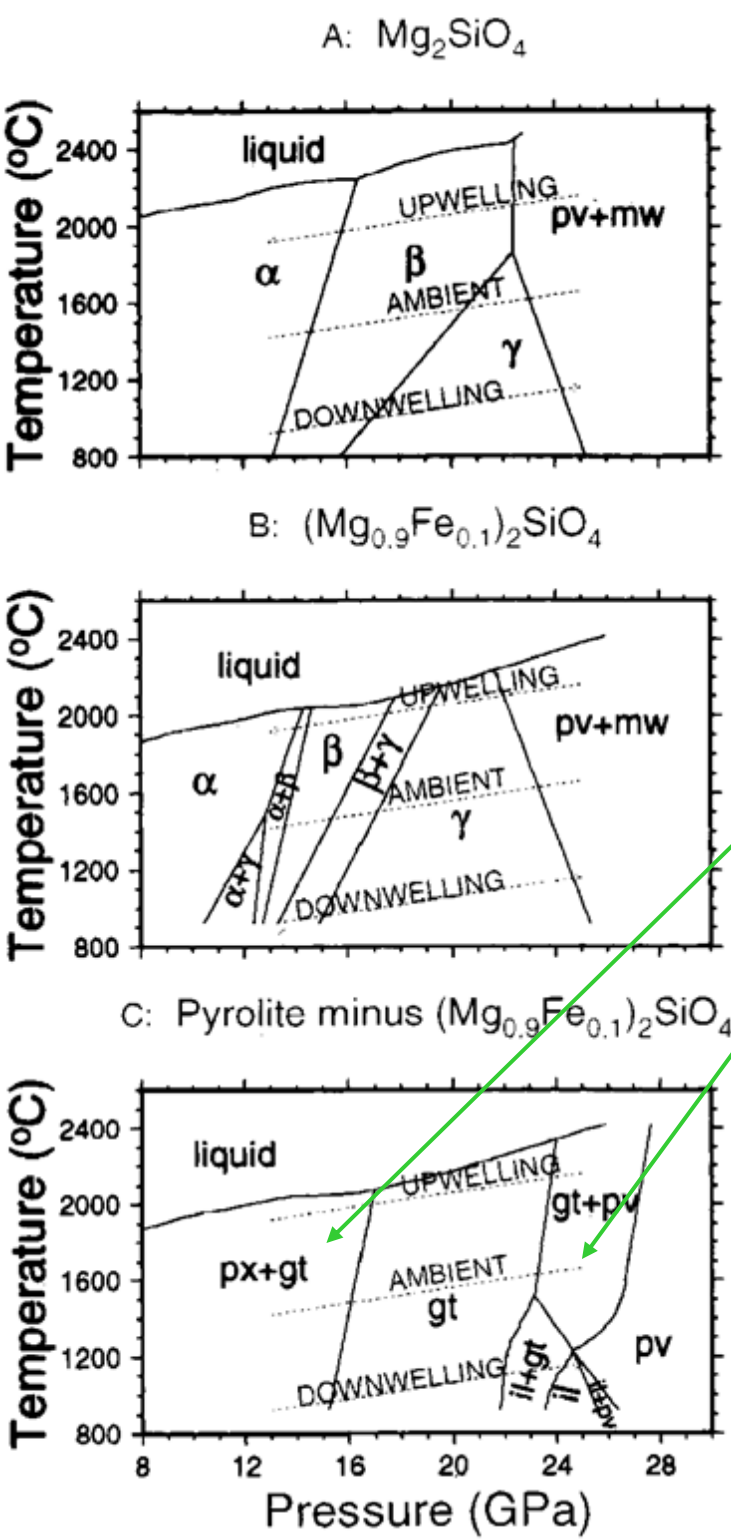


Synthetic seismograms computed through 950°C velocity profile (Fig. 2) of underside SH reflection from the gradient zone at vertical incidence. The pulses have dominant frequencies of 0.2 and 0.05 Hz. Incident pulse minima are aligned on the vertical marker at left. An inferred first-order discontinuity depth may be obtained from the time lag between incidence and reflection. Marker at right shows the 0.05 Hz minimum displaced from that at 0.2 Hz, illustrating the frequency dependence of the time lag, and hence the inferred discontinuity depth.

(Figure 3 of Helffrich and Bina, 1994)

(C.Bina, 9/2011)

Clapeyron Slopes Defined Only for *N=1* Univariant Reactions



These multivariant reactions are too broad to define any meaningful effective Clapeyron slopes for them.

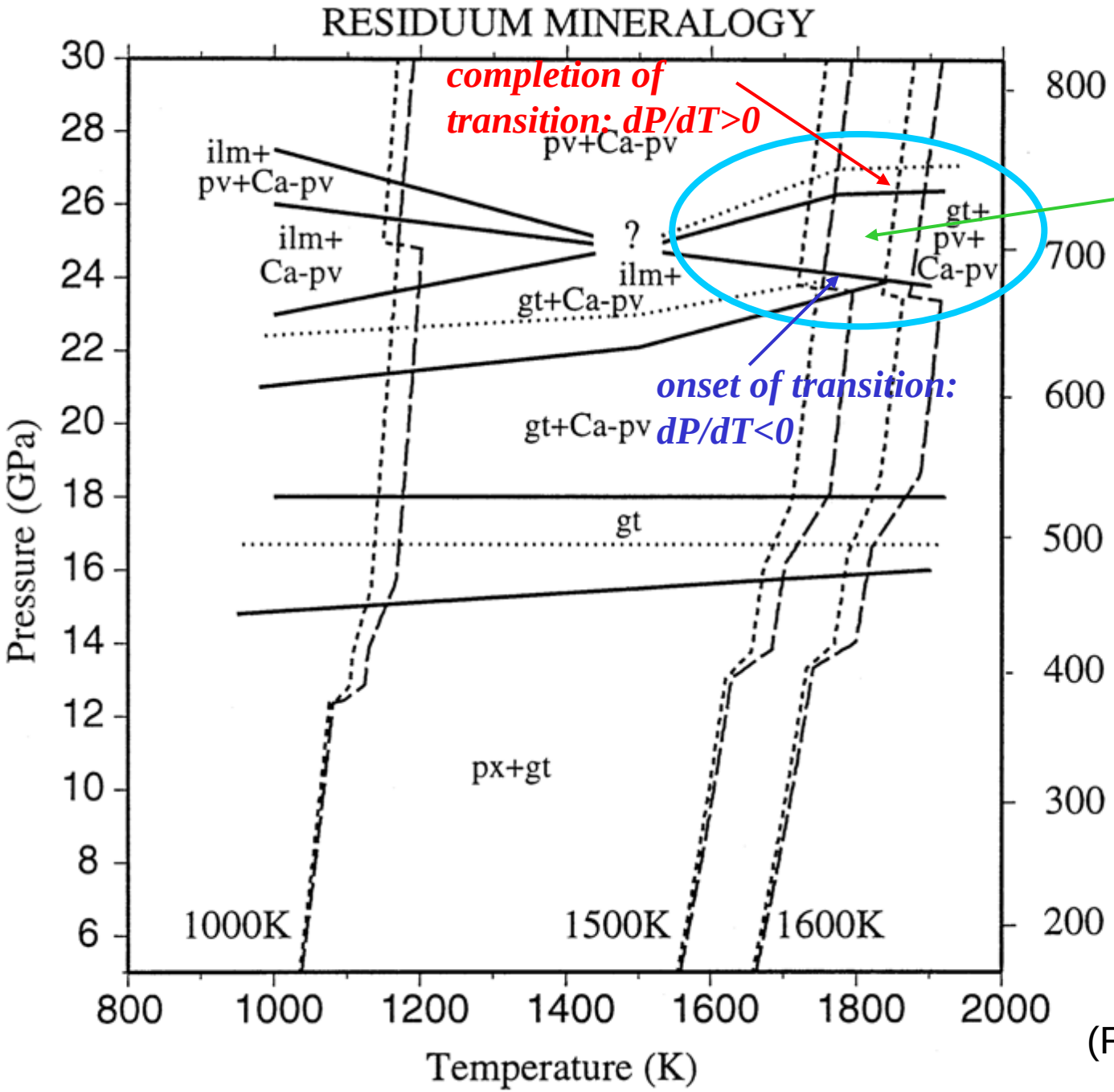
Schematic phase diagrams for Mg_2SiO_4 olivine (**A**), $(Mg_{0.9}Fe_{0.1})_2SiO_4$ olivine (**B**), and pyroxene-garnet components (**C**), after *Gasparik* [I990] and *Ita and Stixrude* [1992]. Phases are olivine (α). modified spinel (β), spinel (γ). perovskite (*pv*), magnesiowüstite (*mw*), pyroxene (*px*), garnet (*gt*) . and ilmenite (*il*). Broken lines depict highlv schematic geotherms for ambient mantle, cold downwellings, and hot upwellings.

(Figure 1 of Bina and Liu, 1995)

(C.Bina, 9/2011)

garnet → silicate perovskite transition

Clapeyron Slopes Defined Only for *N=1* Univariant Reactions



*We cannot even define a meaningful **sign** for a Clapeyron slope for this gt→pv transition in pyrolite.*

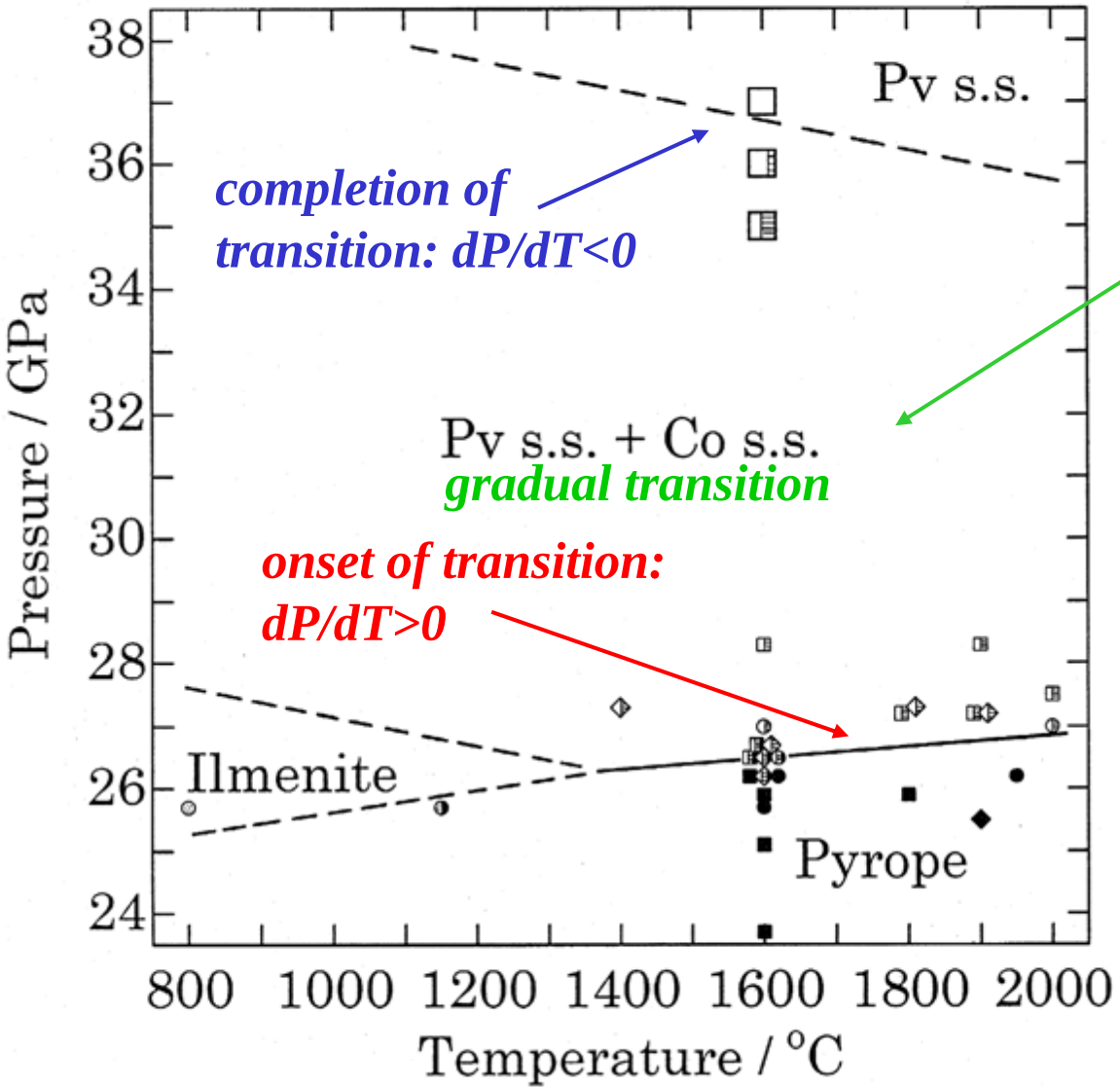
Mineralogy of the residuum components, after Ita and Stixrude (1992). Solid curves correspond to phase boundaries in a pyrolite composition, dotted curves correspond to phase boundaries in a piclogite composition. The adiabats initiated at 1000, 1500 and 1600 K are shown for pyrolite (long dashed lines) and piclogite (short dashed lines). px: pyroxenes; gt: garnets; Ca-pv: Ca-perovskite; ilm: ilmenite; pv: perovskite.

(Figure 2 of Vacher et al., 1998)

(C.Bina, 9/2011)

garnet → silicate perovskite transition

Clapeyron Slopes Defined Only for *N=1* Univariant Reactions



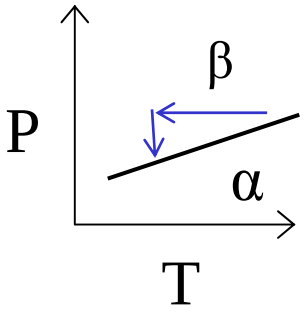
(Figure 5 of Kubo and Akaogi, 2000)

Again, we cannot even define a meaningful ***sign*** *for a Clapeyron slope for this gt→pv transition in pyrope.*

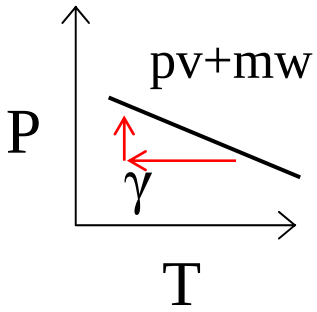
Phase relation of $Mg_3Al_2Si_3O_{12}$ up to 37 GPa. Large squares indicate results by Ito et al. (1998). Small symbols are based on this study. Circular, square and rhombus symbols indicate runs using starting materials of glass, pyrope, and hydrous mixture, respectively. Solid, open, dotted and lined symbols indicate product phases of garnet, perovskite, ilmenite and corundum, respectively. Dashed lines are estimated boundaries. Abbreviations: Pv, perovskite; Co, corundum; Il, ilmenite; s.s., solid solution.

(C.Bina, 9/2011)

Clapeyron Slopes and Convection

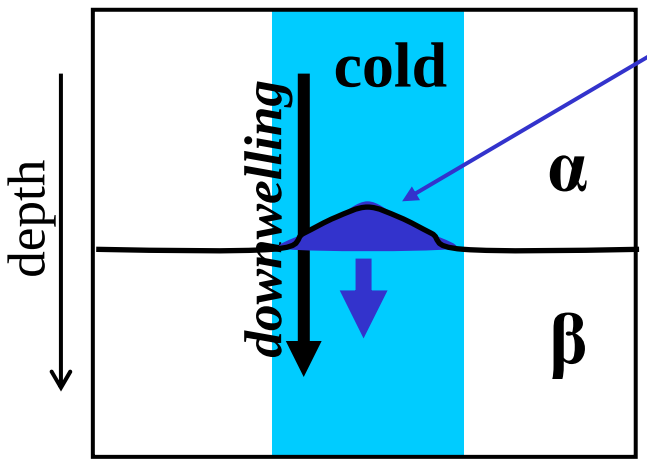


dP/dT > 0

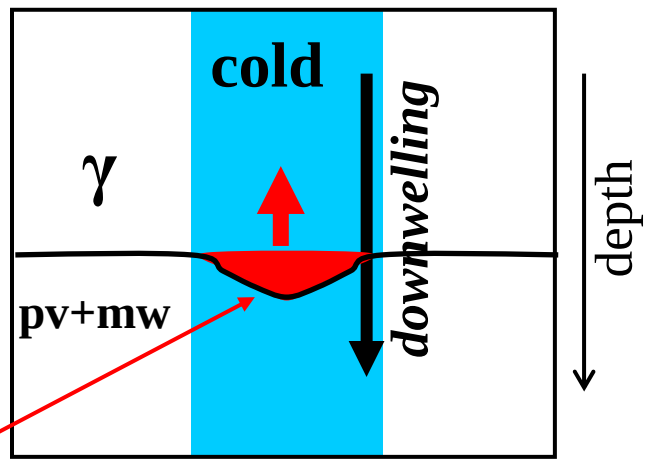


dP/dT < 0

β more dense than surrounding α;
negative buoyancy promotes downwelling



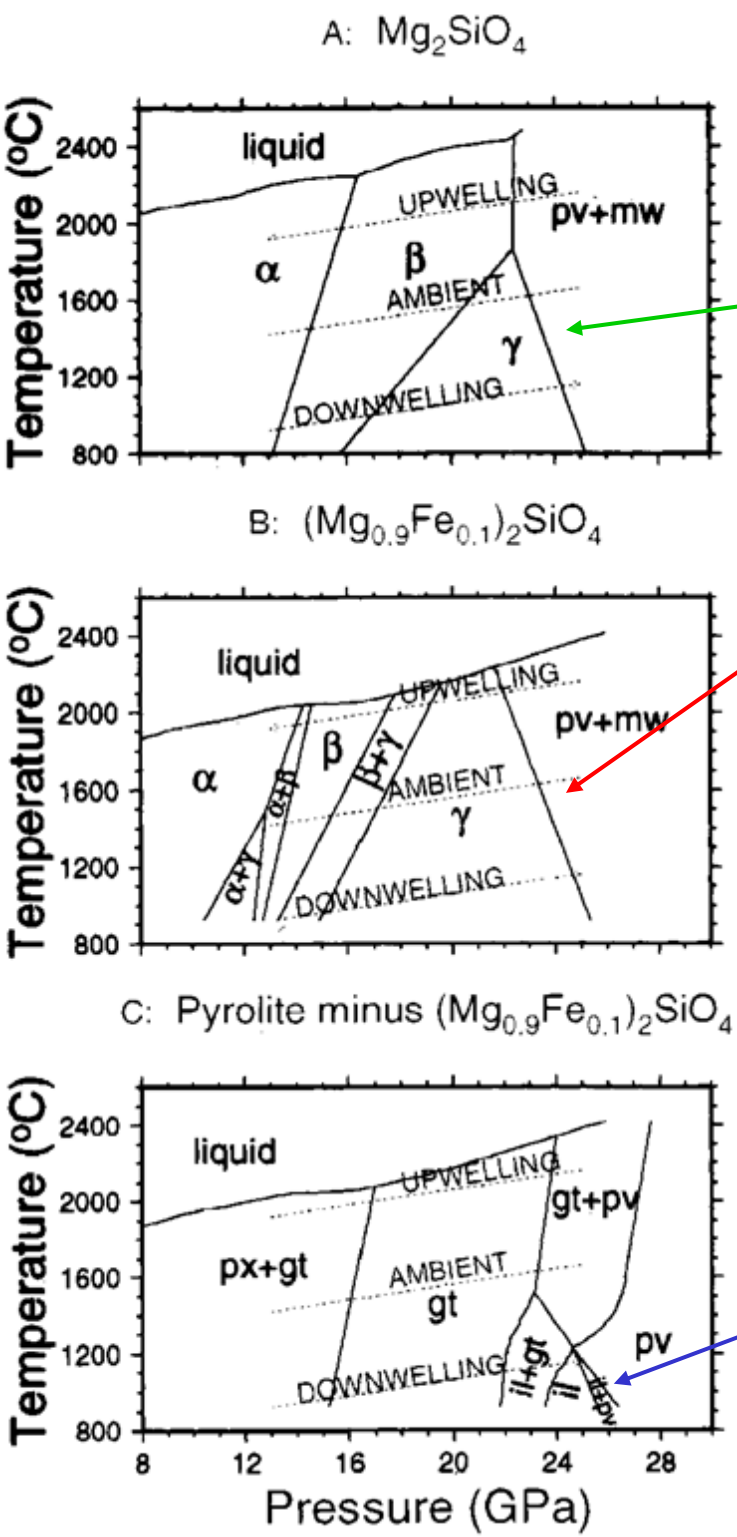
γ less dense than surrounding pv+mw;
positive buoyancy inhibits downwelling



(cf. Christensen and Yuen, 1984, 1985)

(C.Bina, 9/2011)

Clapeyron Slopes and Convection



dP/dT<0 from low to moderate T

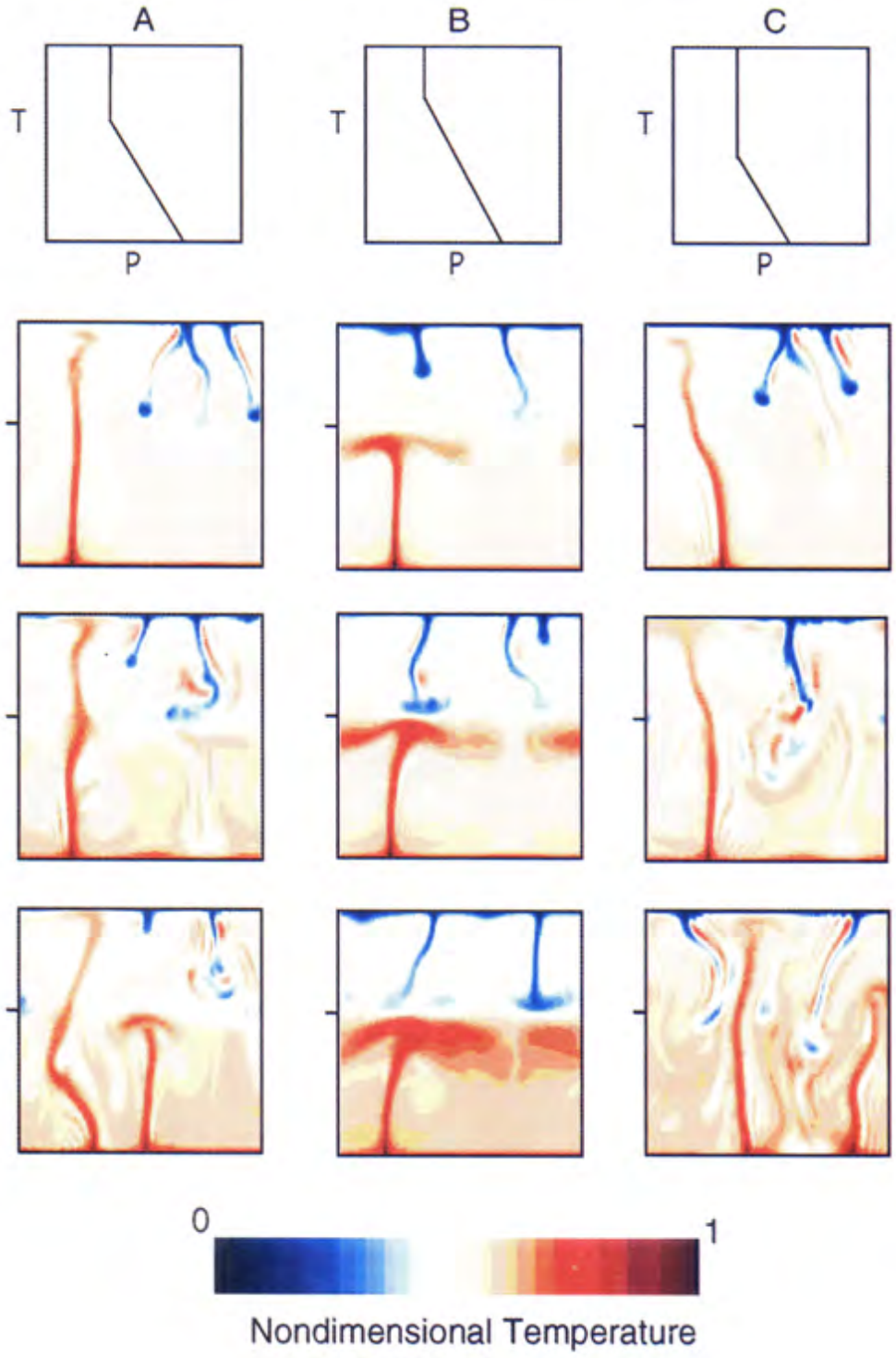
dP/dT<0 from low to high T

dP/dT<0 only at low T

Schematic phase diagrams for Mg_2SiO_4 olivine (**A**), $(Mg_{0.9}Fe_{0.1})_2SiO_4$ olivine (**B**), and pyroxene-garnet components (**C**), after *Gasparik* [I990] and *Ita and Stixrude* [1992]. Phases are olivine (α). modified spinel (β), spinel (γ). perovskite (*pv*), magnesiowüstite (*mw*), pyroxene (*px*), garnet (*gt*) . and ilmenite (*il*). Broken lines depict highlv schematic geotherms for ambient mantle, cold downwellings, and hot upwellings.

(Figure 1 of Bina and Liu, 1995)

(C.Bina, 9/2011)



A: slabs stagnate; plumes penetrate

B: separated two-layer convection

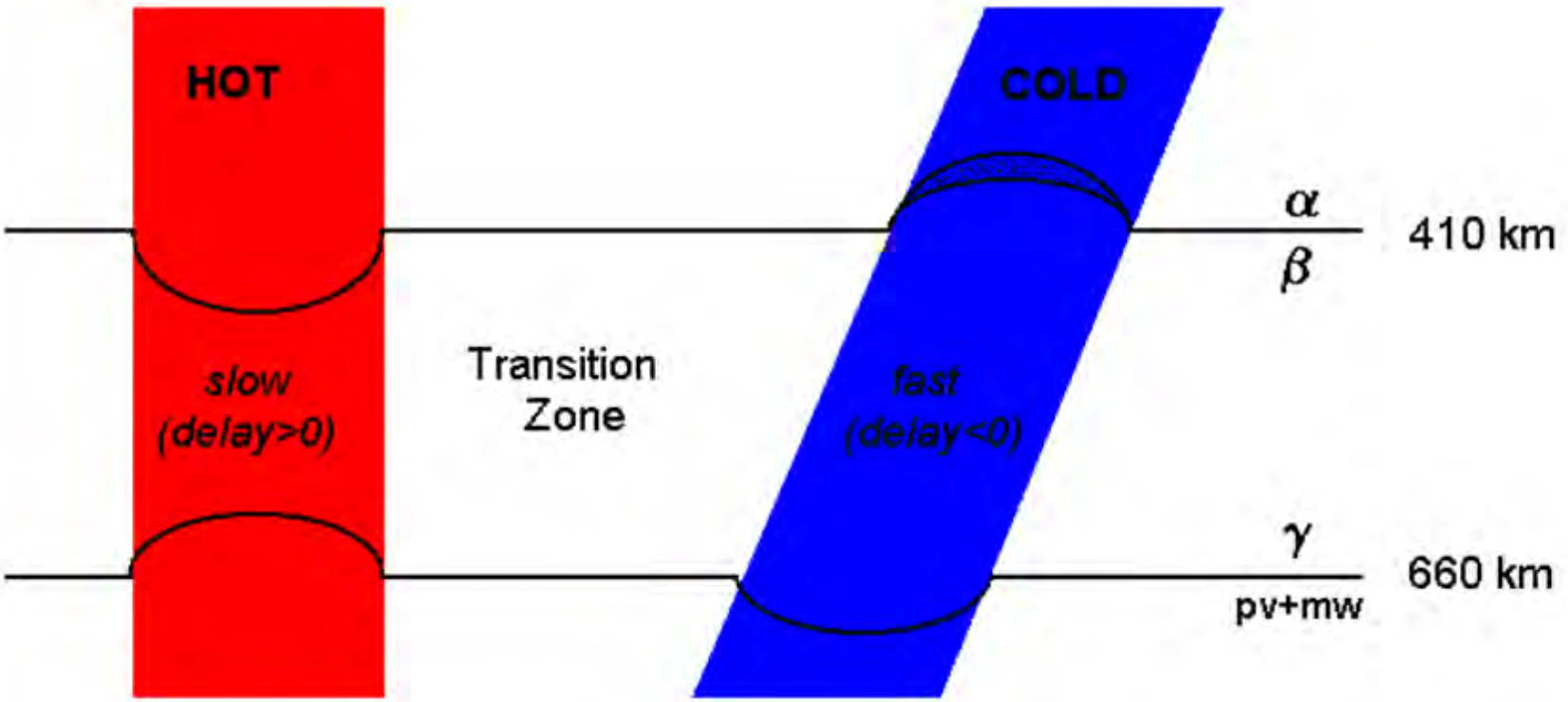
C: plumes penetrate; slabs entrained

Numerically simulated evolution of mantle thermal field for three phase diagram topologies. Phase transitions change Clapeyron slope from −4 to 0 MPa/K above 1800°C (**A**), 2100°C (**B**), or 1350°C (**C**). Rayleigh number in all cases is 1×10^6**.** Tick marks indicate 660 km depth. Aspect ratio is three (horizontal) to one (vertical). Images in each column are sequential snapshots of thermal field. Top panels: beginning of experiment, convection has gone through one overturn. Middle panels: after two to three overturns. Bottom panels: after four to five overturns.

(Figure 2 of Bina and Liu, 1995)

(C.Bina, 9/2011)

Clapeyron Slopes and Seismic Structure

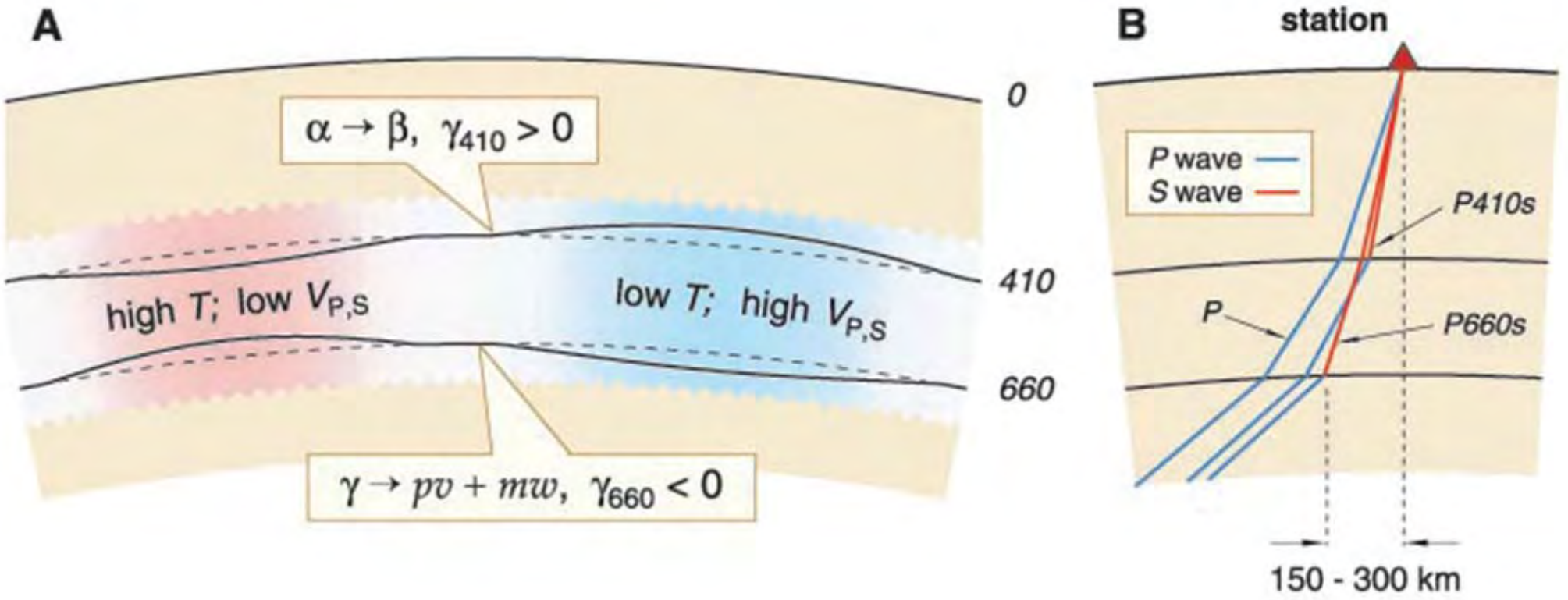


Schematic illustration of thermal control of olivine phase transformations in the transition zone, showing perturbations to transition zone thickness, transition zone seismic velocities (delay times), and depths of individual phase transformations.

(Figure 2 of Bina [2003])

Clapeyron Slopes and Seismic Structure

a seismological experiment

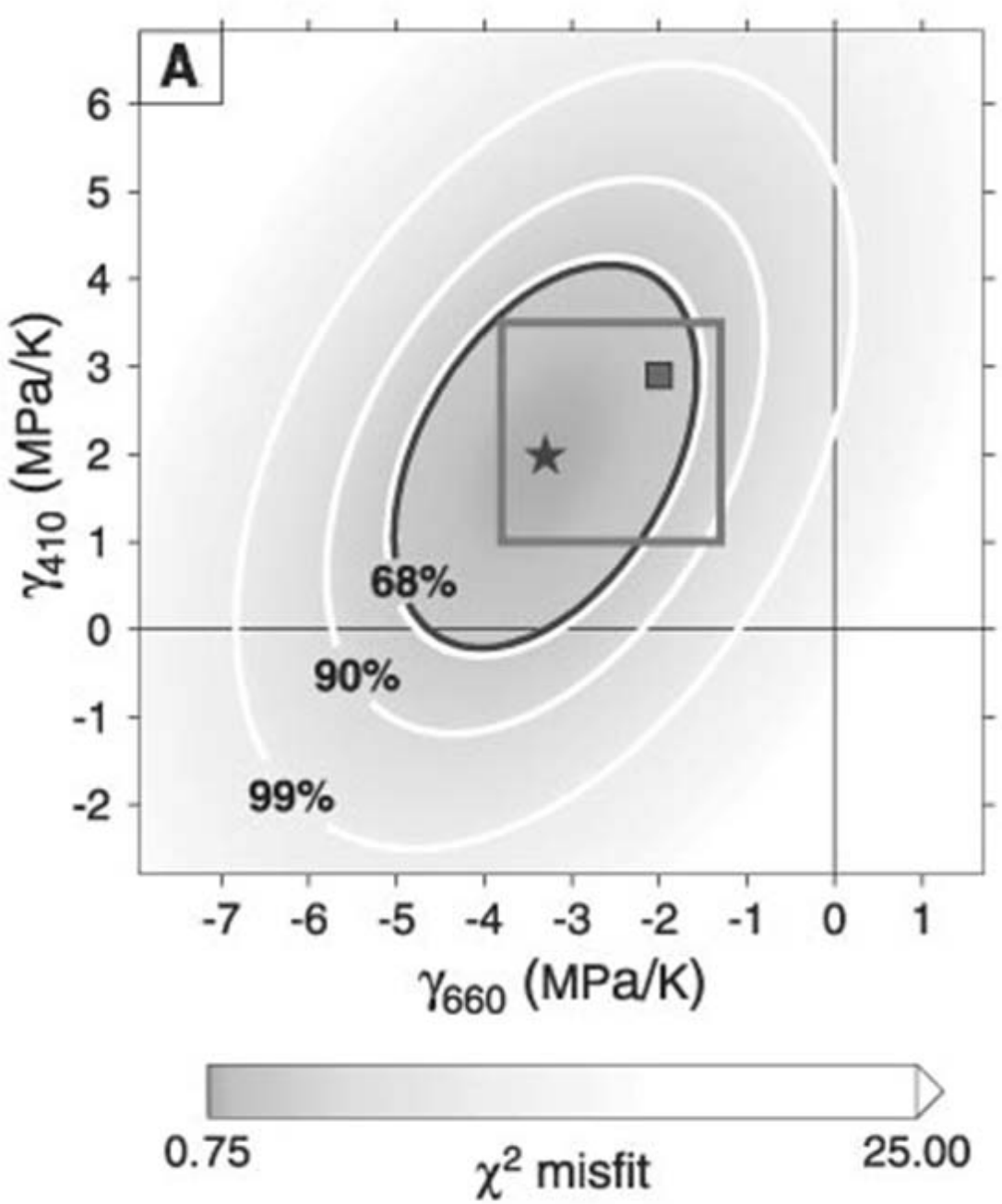


(**A**) Schematic depiction of the transition zone in an olivine-dominant mantle. The α→β and γ→*pv*+*mw* phase transformations give rise to the 410- and 660-km discontinuities, and the effective Clapeyron slopes γ_{410} and γ_{660} have opposite signs. Absent lateral variations in composition, relatively low temperatures (*T*) cause thickening of the TZ and increase in seismic velocities (V_P, V_S); high temperatures cause thinning of the TZ and decrease in $V_{P,S}$. (**B**) Schematic ray diagram of the *P*, *P*410*s*, and *P*660*s* phases.

(Figure 1 of Lebedev et al. [2002])

(C.Bina, 9/2011)

Clapeyron Slopes and Seismic Structure



Observed seismic topography matches experimental slopes.

(**A**) The effective Clapeyron slopes at the 410- and 660-km discontinuities. χ^2 misfit in the γ_{410}-γ_{660} plane is plotted in the region around the best-fit solution (star). The values of the mineralogical Clapeyron slopes of $\alpha \rightarrow \beta$ and $\gamma \rightarrow pv+mw$ from (*14*) [small solid square at (22.0 MPa; 2.9 MPa)] and the range of measured values from the literature as compiled in (*14*) (large rectangle) are superimposed as γ_{410} and γ_{660}.

(Figure 2a of Lebedev et al. [2002])

(C.Bina, 9/2011)

EXO/ENDO-THERMIC REACTIONS

At equilibrium: $\Delta G^{\alpha\to\beta} = \Delta H^{\alpha\to\beta} - T\Delta S^{\alpha\to\beta} = 0$

$\Rightarrow \Delta H^{\alpha\to\beta} = T\Delta S^{\alpha\to\beta}$

heat transfer

EXO/ENDO-THERMIC REACTIONS

At equilibrium: $\Delta G^{\alpha\to\beta} = \Delta H^{\alpha\to\beta} - T\Delta S^{\alpha\to\beta} = 0$

$\Rightarrow \Delta H^{\alpha\to\beta} = T\Delta S^{\alpha\to\beta}$

High-P subsolidus transformation:

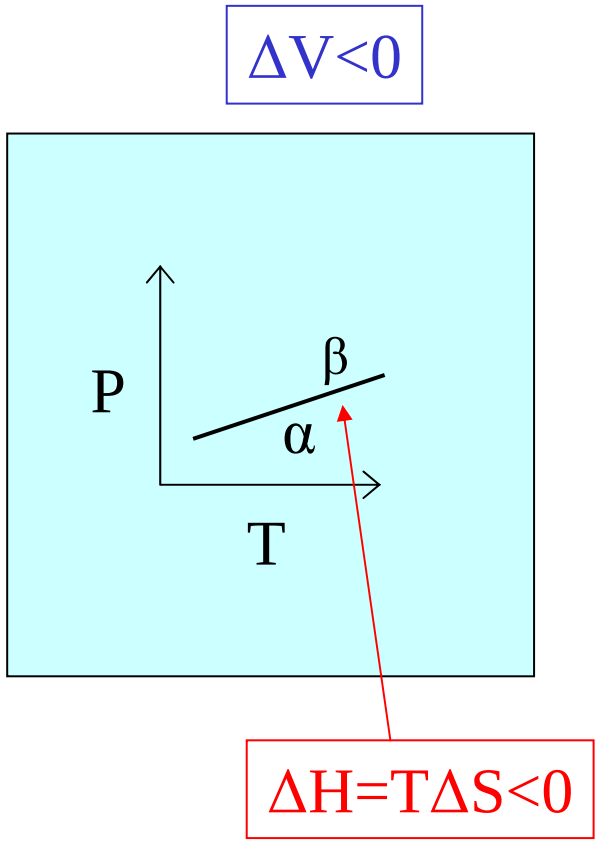
Positive Clapeyron slope (+):

$$\frac{dP}{dT} = \frac{\Delta S^{\alpha\to\beta}(P,T)}{\Delta V^{\alpha\to\beta}(P,T)} > 0$$

$\Delta V^{\alpha\to\beta} < 0$ [solid $\to$ denser]

$\Rightarrow \Delta S^{\alpha\to\beta} < 0 \Rightarrow \Delta H^{\alpha\to\beta} < 0$

[Exothermic ("out-heat")]



(C.Bina, 9/2011)

EXO/ENDO-THERMIC REACTIONS

At equilibrium: $\Delta G^{\alpha\to\beta} = \Delta H^{\alpha\to\beta} - T\Delta S^{\alpha\to\beta} = 0$

$\Rightarrow \Delta H^{\alpha\to\beta} = T\Delta S^{\alpha\to\beta}$

High-P subsolidus transformation:

Positive Clapeyron slope (+):

$$\frac{dP}{dT} = \frac{\Delta S^{\alpha\to\beta}(P,T)}{\Delta V^{\alpha\to\beta}(P,T)} > 0$$

$\Delta V^{\alpha\to\beta} < 0$ [solid $\to$ denser]

$\Rightarrow \Delta S^{\alpha\to\beta} < 0 \Rightarrow \Delta H^{\alpha\to\beta} < 0$

[Exothermic ("out-heat")]

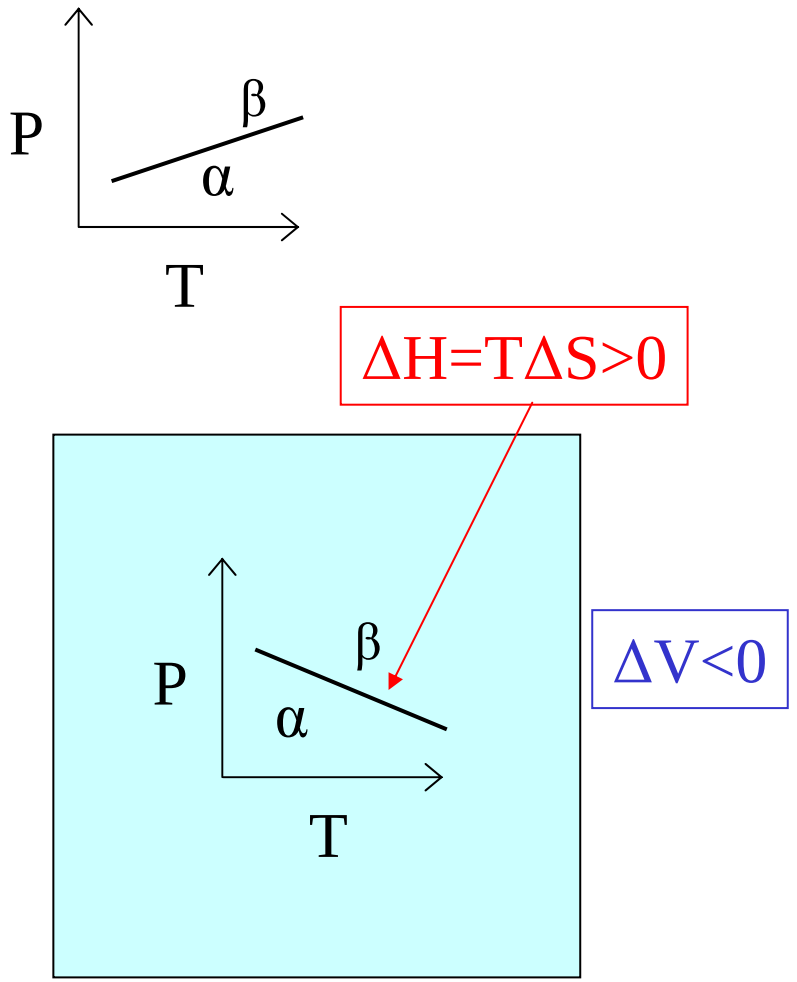
Negative Clapeyron slope (−):

$$\frac{dP}{dT} = \frac{\Delta S^{\alpha\to\beta}(P,T)}{\Delta V^{\alpha\to\beta}(P,T)} < 0$$

$\Delta V^{\alpha\to\beta} < 0$ [solid $\to$ denser]

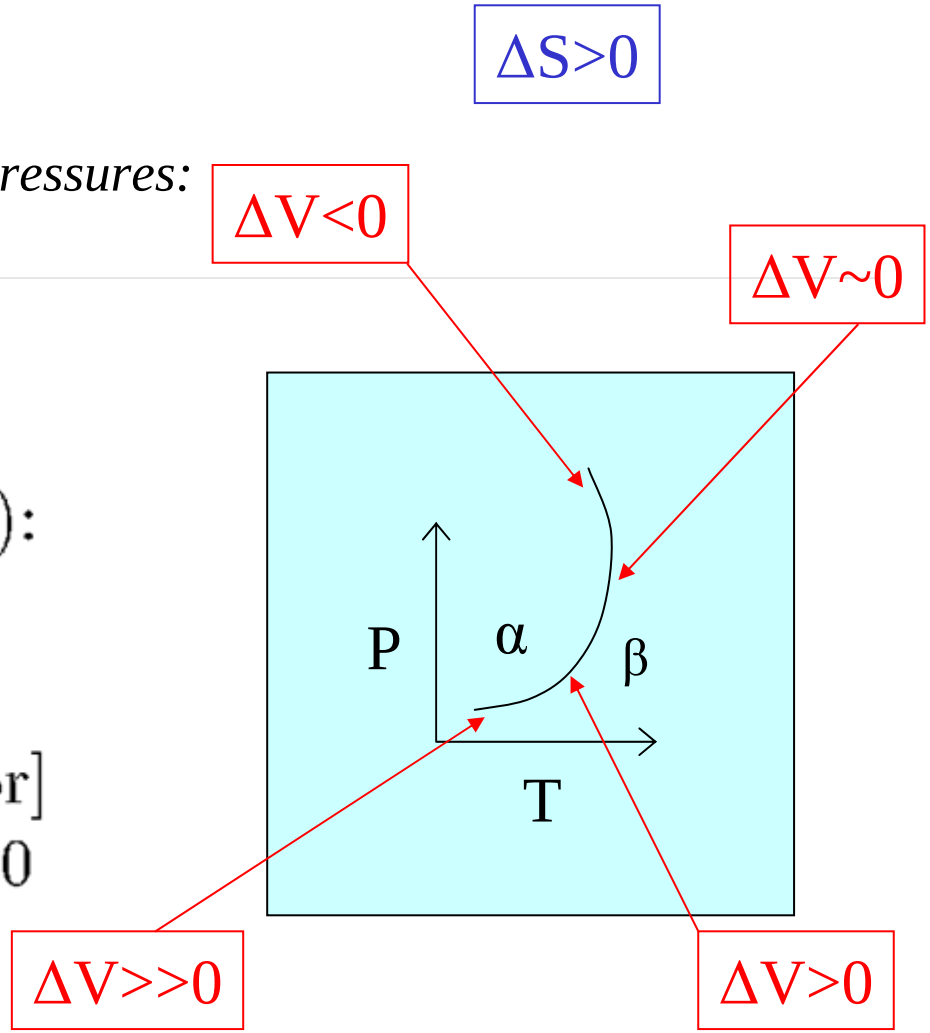
$\Rightarrow \Delta S^{\alpha\to\beta} > 0 \Rightarrow \Delta H^{\alpha\to\beta} > 0$

[Endothermic ("in-heat")]



(C.Bina, 9/2011)

At higher pressures:



High-T dehydration reaction:

Positive Clapeyron slope (+):

$$\frac{dP}{dT} = \frac{\Delta S^{\alpha\to\beta}(P,T)}{\Delta V^{\alpha\to\beta}(P,T)} > 0$$

$\Delta V^{\alpha\to\beta} > 0$ [solid $\to$ vapor]

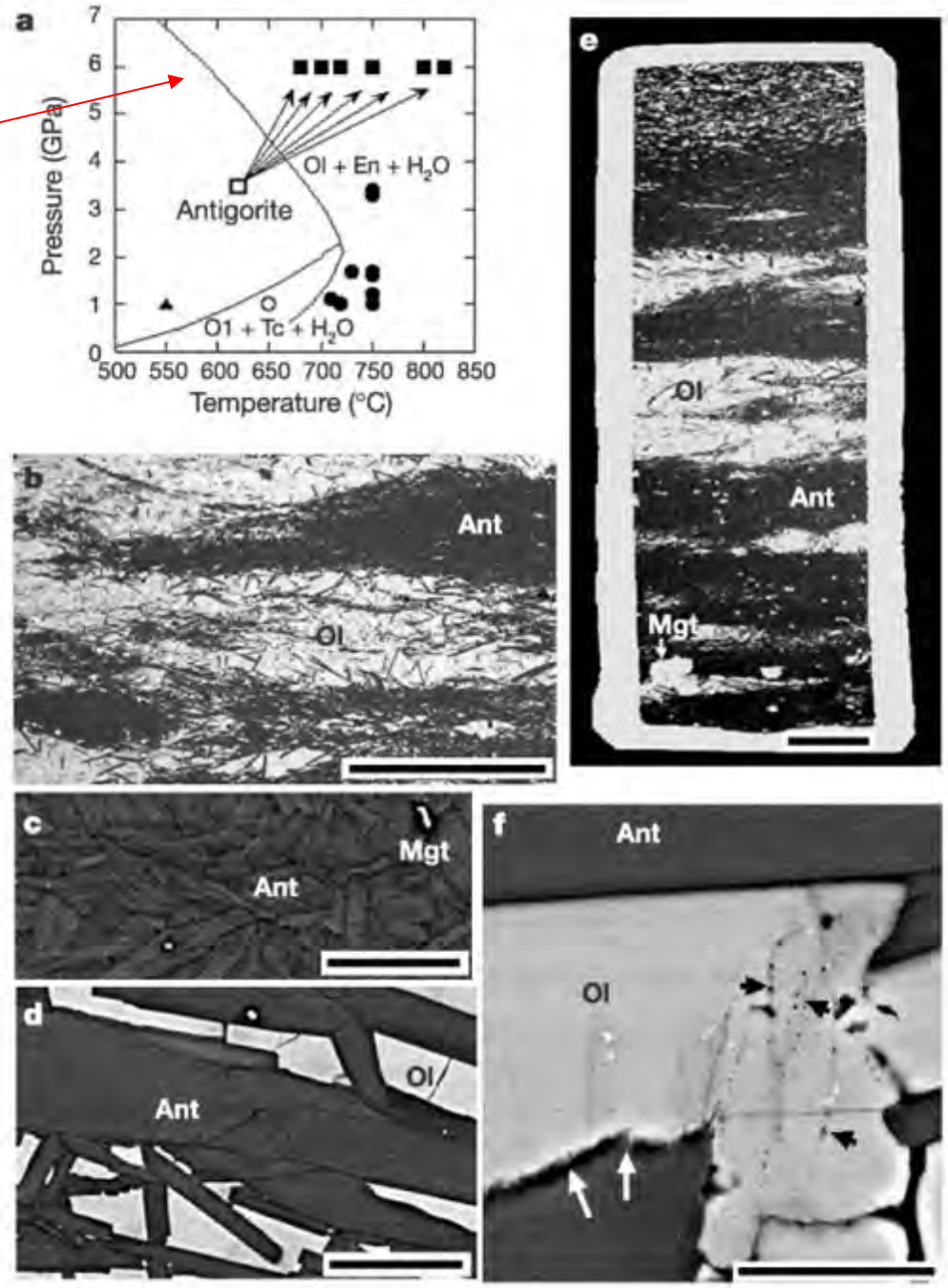
$\Rightarrow \Delta S^{\alpha\to\beta} > 0 \Rightarrow \Delta H^{\alpha\to\beta} > 0$

[Endothermic ("in-heat")]

[Note: Vapors are more compressible than solids, so that as P increases, $\Delta V^{\alpha\to\beta}$ decreases, and $\frac{dP}{dT}$ grows steeper.]

Dehydration Reactions at High Pressures

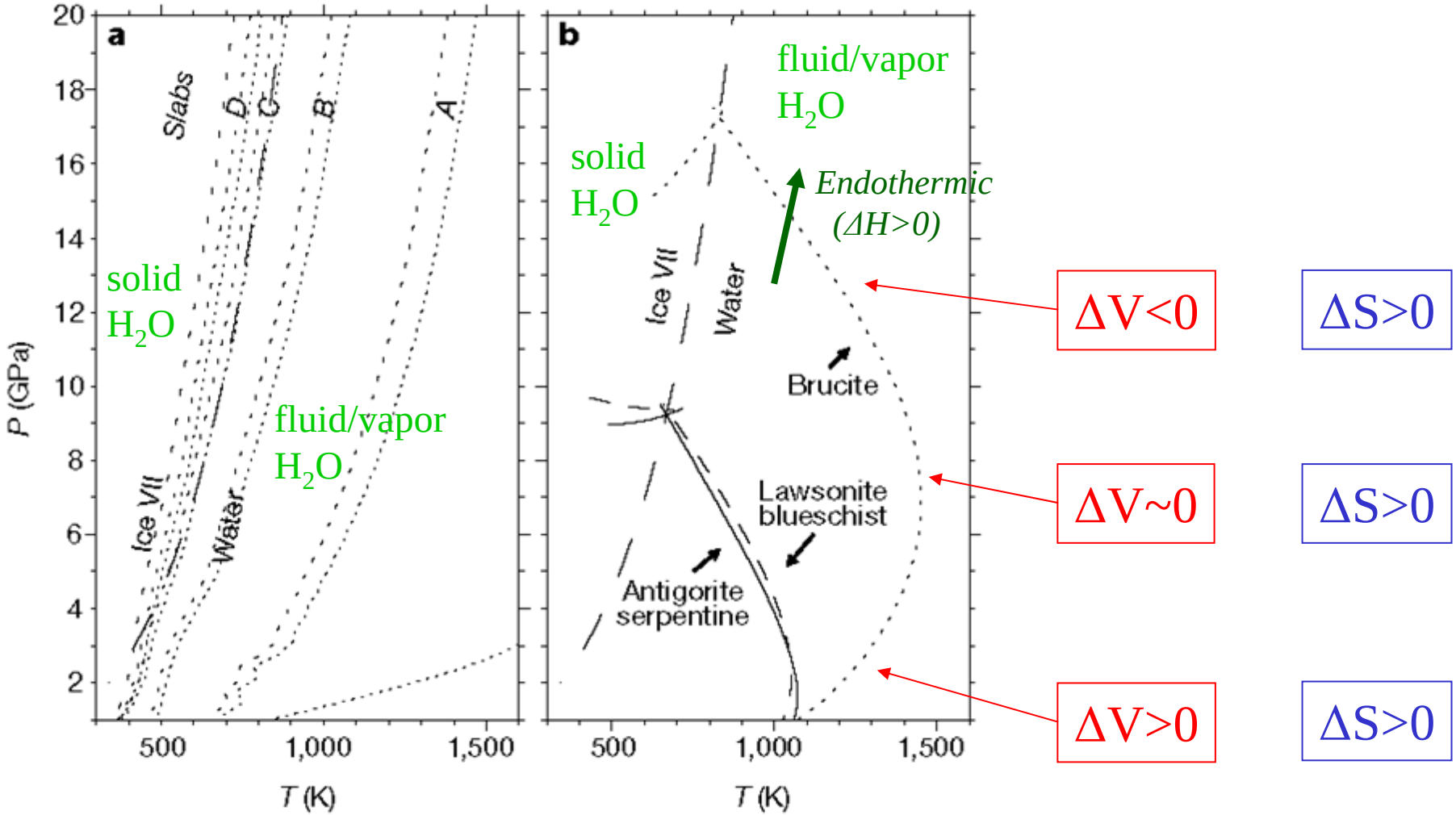
$\Delta V<0$



(Figure 2 of Jung, Green, and Dobrzhinetskaya, 2004, "Intermediate-depth earthquake faulting by dehydration embrittlement with negative volume change")

(C.Bina, 9/2011)

Dehydration Reactions at High Pressures and at Low Temperatures

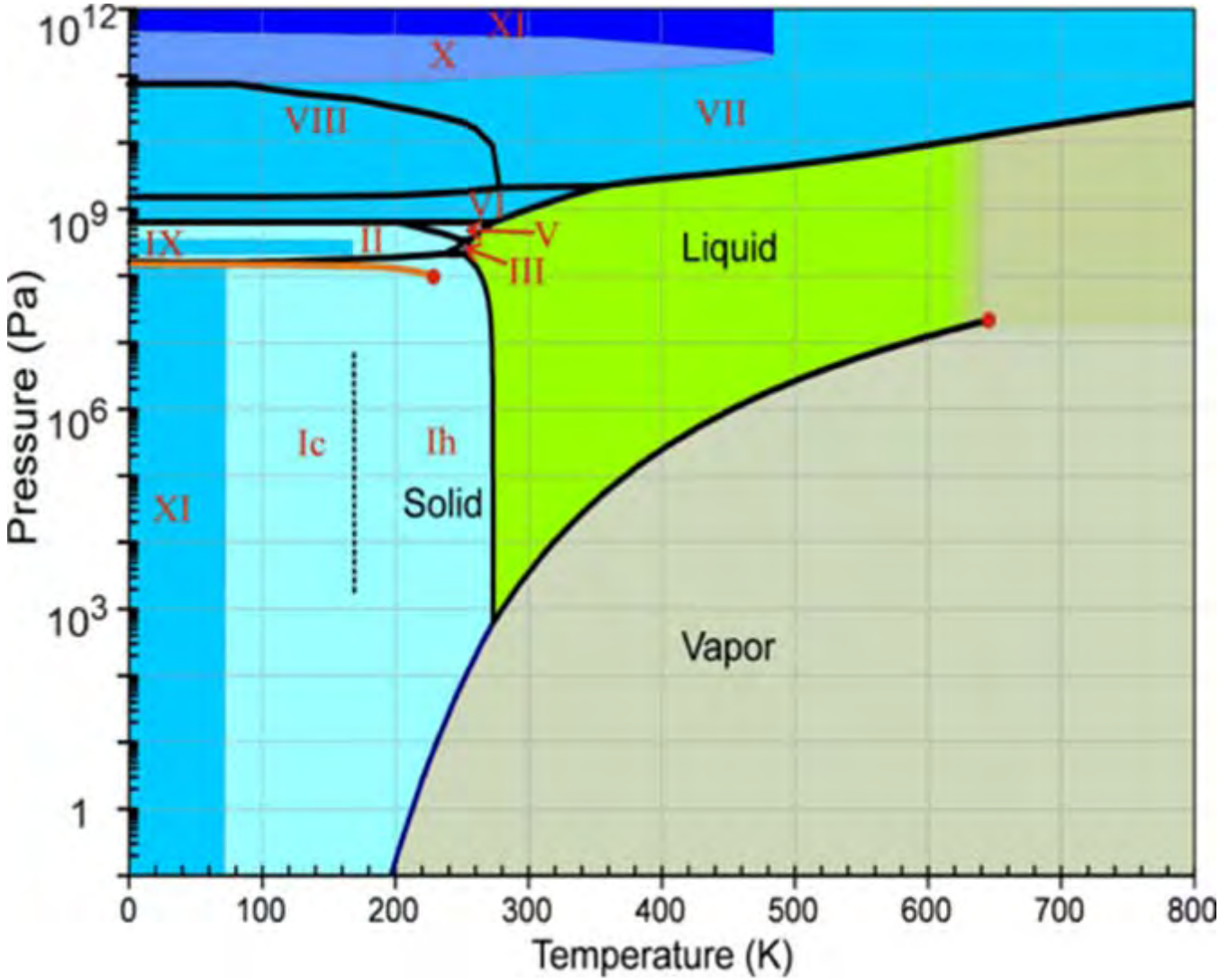


The melting curve of ice VII. Data from experimental measurements of melting conditions. Heavy dashed line shows the melting curve. **a**, Superimposed are the minimum temperatures inside slabs, calculated for a range of subduction zone thermal models (slab classes *A, B, C* and *D*) along with a typical mantle geotherm (dotted lines). **b**, Superimposed are calculated equilibrium reaction boundaries for three representative dehydration reactions: *brucite to periclase* (dotted lines), *lawsonite blueschist to quartz eclogite* (dashed lines), and *antigorite (serpentine) to enstatite plus phase A* (solid lines).

(Figure 1 of Bina and Navrotsky, 2000)

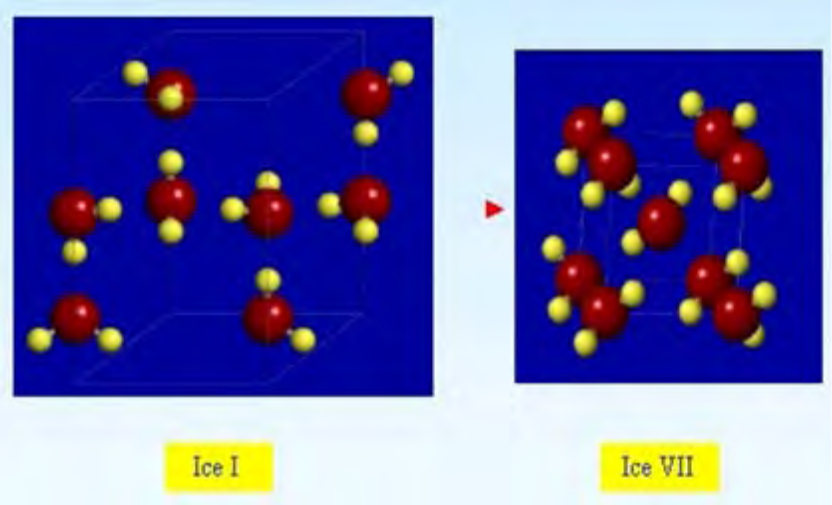
(C.Bina, 9/2011)

Phase Diagram of H_2O



(diagram by M. Chaplin)

(C.Bina, 9/2011)

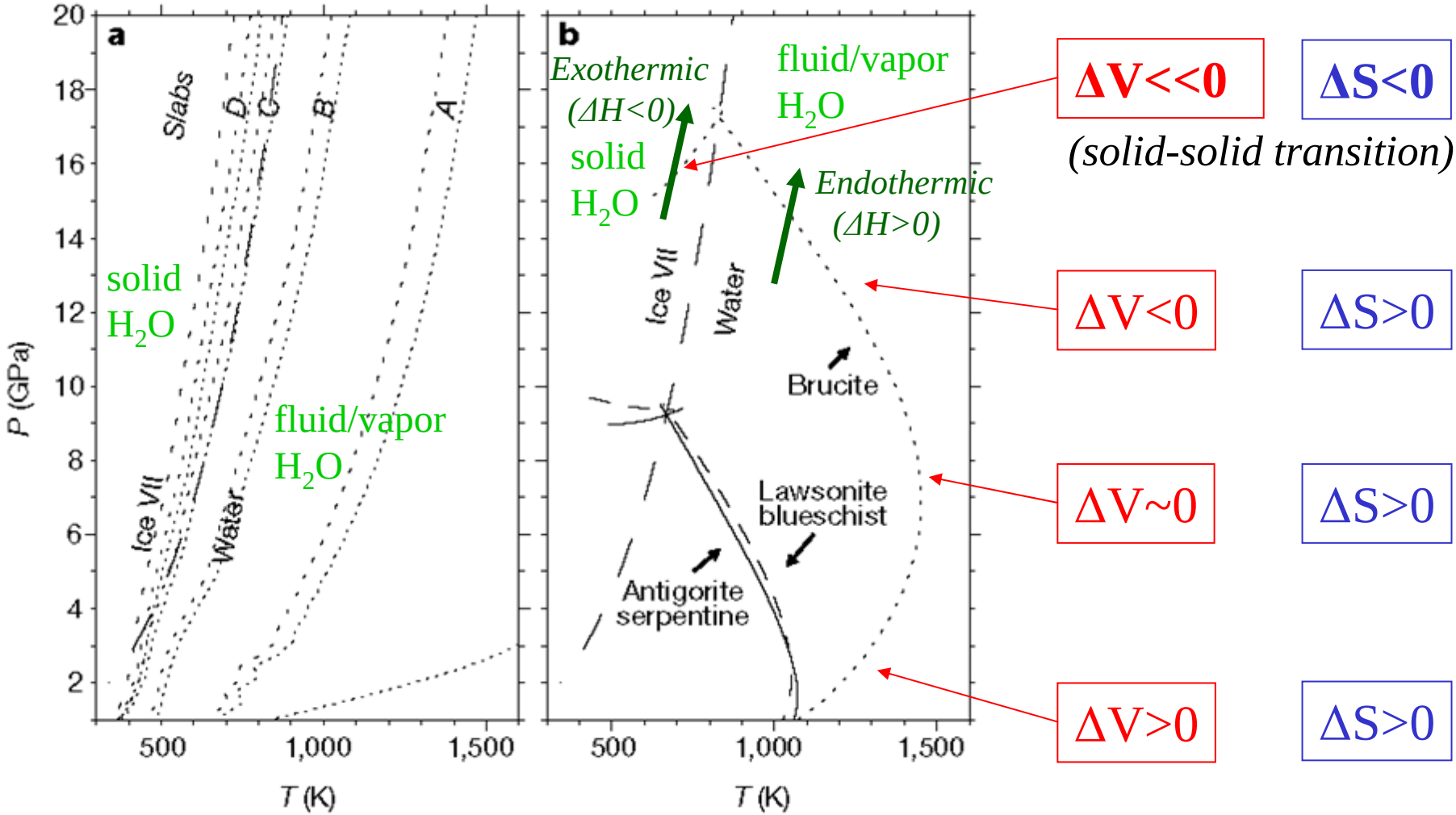


(structures by R. Hemley)



(photo by T. Yagi)

Dehydration Reactions at High Pressures and at Low Temperatures



The melting curve of ice VII. Data from experimental measurements of melting conditions. Heavy dashed line shows the melting curve. **a**, Superimposed are the minimum temperatures inside slabs, calculated for a range of subduction zone thermal models (slab classes *A, B, C* and *D*) along with a typical mantle geotherm (dotted lines). **b**, Superimposed are calculated equilibrium reaction boundaries for three representative dehydration reactions: *brucite to periclase* (dotted lines), *lawsonite blueschist to quartz eclogite* (dashed lines), and *antigorite (serpentine) to enstatite plus phase A* (solid lines).

(Figure 1 of Bina and Navrotsky, 2000)

(C.Bina, 9/2011)

EXO/ENDO-THERMIC REACTIONS

direction of reaction

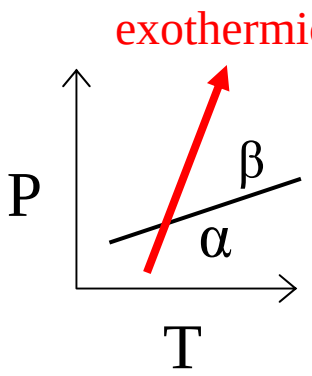
At equilibrium: $\Delta G^{\alpha\to\beta} = \Delta H^{\alpha\to\beta} - T\Delta S^{\alpha\to\beta} = 0$
$\Rightarrow \Delta H^{\alpha\to\beta} = T\Delta S^{\alpha\to\beta}$

High-P subsolidus transformation:

Positive Clapeyron slope (+):

$\frac{dP}{dT} = \frac{\Delta S^{\alpha\to\beta}(P,T)}{\Delta V^{\alpha\to\beta}(P,T)} > 0$

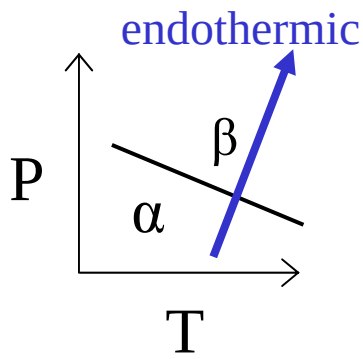
$\Delta V^{\alpha\to\beta} < 0$ [solid → denser]
$\Rightarrow \Delta S^{\alpha\to\beta} < 0 \Rightarrow \Delta H^{\alpha\to\beta} < 0$
[Exothermic ("out-heat")]



Negative Clapeyron slope (−):

$\frac{dP}{dT} = \frac{\Delta S^{\alpha\to\beta}(P,T)}{\Delta V^{\alpha\to\beta}(P,T)} < 0$

$\Delta V^{\alpha\to\beta} < 0$ [solid → denser]
$\Rightarrow \Delta S^{\alpha\to\beta} > 0 \Rightarrow \Delta H^{\alpha\to\beta} > 0$
[Endothermic ("in-heat")]

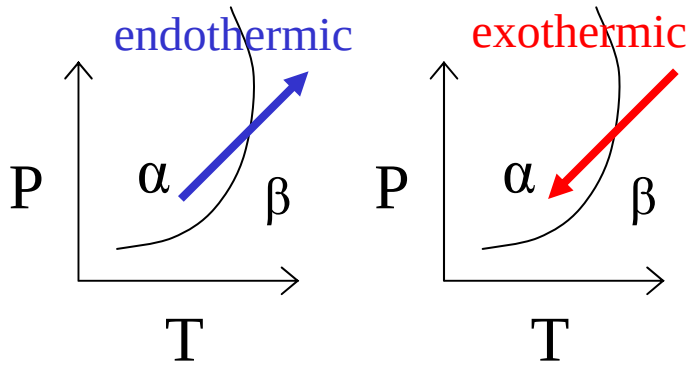


High-T dehydration reaction:

Positive Clapeyron slope (+):

$\frac{dP}{dT} = \frac{\Delta S^{\alpha\to\beta}(P,T)}{\Delta V^{\alpha\to\beta}(P,T)} > 0$

$\Delta V^{\alpha\to\beta} > 0$ [solid → vapor]
$\Rightarrow \Delta S^{\alpha\to\beta} > 0 \Rightarrow \Delta H^{\alpha\to\beta} > 0$
[Endothermic ("in-heat")]



[Note: Vapors are more compressible than solids, so that as P increases, $\Delta V^{\alpha\to\beta}$ decreases, and $\frac{dP}{dT}$ grows steeper.]

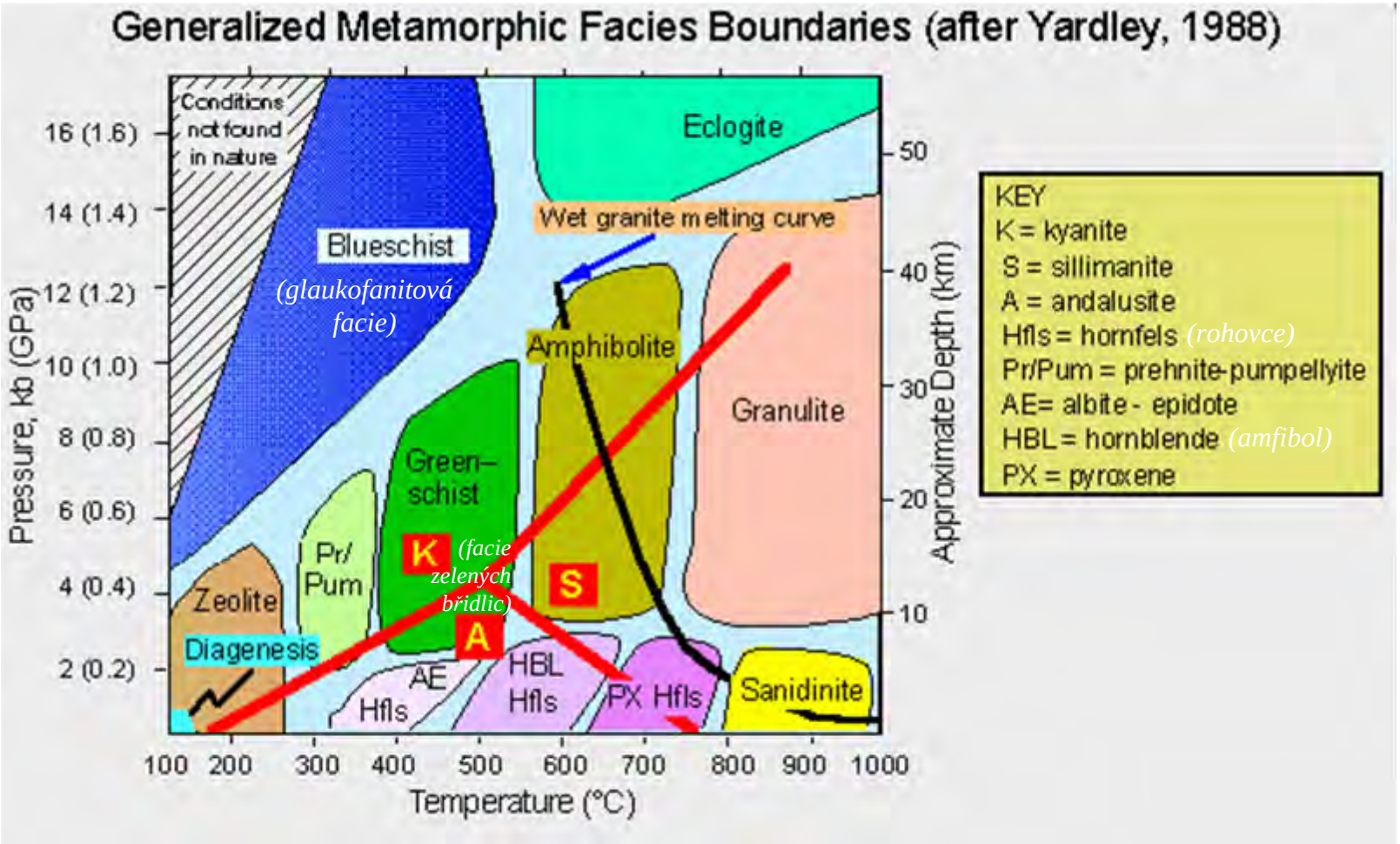
(C.Bina, 9/2011)

Geobarometry and Geothermometry

Petrology allows us to estimate the range of pressure *and* temperature *of equilibration by observing the coexisting mineral species.*

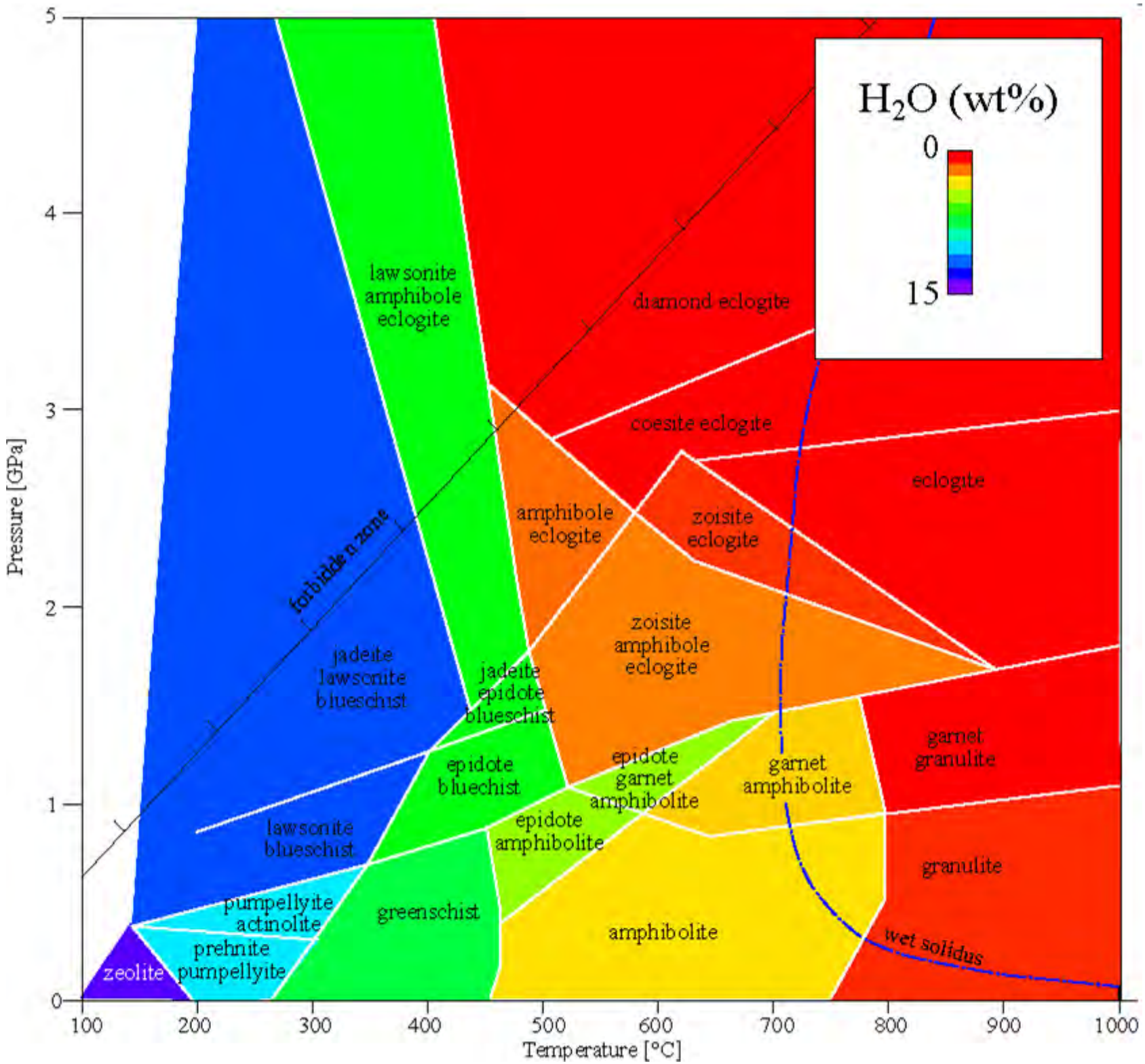
(C.Bina, 9/2011)

metamorfní facie (stupně metamorfózy)



(from J. Ahern)

podrobnější metamorfní facie (stupně metamorfózy)



(from B. Hacker)

(C.Bina, 9/2011)